

## SHOCK WAVES AND NUCLEOSYNTHESIS IN TYPE II SUPERNOVAE

M. B. AUFDERHEIDE AND E. BARON<sup>1</sup>

Department of Physics, State University of New York at Stony Brook, New York, NY 11794-3800

AND

F.-K. THIELEMANN

Harvard-Smithsonian Center for Astrophysics, 60 Garden Street, Cambridge, MA 02138

Received 1990 June 22; accepted 1990 September 18

## ABSTRACT

In the study of nucleosynthesis in Type II supernovae, shock waves are initiated artificially, since collapse calculations do not, as yet, give self-consistent shock waves strong enough to produce the supernova explosion. We study the two different initiation methods currently used by light-curve modelers. In particular, we focus on the peak temperatures and the nucleosynthetic yields in each method. We discuss the various parameters involved in artificially initiating a shock wave and examine the effects of varying these parameters. We discuss the implications of this for the total nickel mass ejected from the star, the primary observable, as well as the general nucleosynthesis pattern of intermediate-mass elements, emerging from the explosion.

*Subject headings:* nucleosynthesis — shock waves — stars: supernovae

## 1. INTRODUCTION

It has been known for more than 30 years that the prodigious pyrotechnics associated with Type II supernovae are caused by the propagation of a shock wave from the core of the star out to its surface. What has still not been discovered is how to produce a shock wave with enough energy to power the supernova (see, however, recent results of Mayle & Wilson 1990). Fortunately, many features of supernovae are relatively insensitive to the actual mechanism by which the shock is powered. One such feature is the optical display of the supernova. In the case of SN 1987A, the shock wave had to smash through more than  $10 M_{\odot}$  of matter before reaching the photosphere. Propagation through this much material certainly washes out all information about the supernova mechanism, except for the fact that such a mechanism exists. Indeed, the hydrogen mantle of such a supergiant has a self-similar density profile, and the shock's history there can be modeled by a Sedov solution (Sedov 1959). In such a case, the shock's effect on the mantle will be determined only by the amount of energy deposited by the shock wave.

The whole star does not obey a single similarity law, however. The star's structure is complicated by the presence of entropy and composition gradients caused by shell burning. Such gradients lead to a density profile which is only self-similar in pieces. Thus, events which occur just outside the iron core may still bear enough features of the shock wave to be able to provide some information about the supernova mechanism. In this region the important radioactive element  $^{56}\text{Ni}$ , as well as the intermediate-mass elements (Si-Ca) are produced. This material is produced by burning as the shock wave passes through the mantle. Because the mass of the resulting neutron star is not known, it is not clear where the mass cut is in the presupernova star. Thus, it is not possible to determine exactly where in the progenitor the newly produced nickel originated.

If we wish to study the explosive processing of elements in the silicon, oxygen, neon, carbon, and helium shells, we are

forced to generate a shock wave somewhere within these regions which will give the proper optical display. This method is not self-consistent, but it does allow the study of the explosive nucleosynthesis as a function of the energy dumped into the star. There are many different ways to initiate a shock wave within such a presupernova model, however. In this paper we study how this choice affects the explosive nucleosynthesis. In §§ 2 and 3 the methods used to generate and compare shock waves are discussed. In § 4 the temperature profiles generated by various kinds of initiation methods are discussed. In § 5 the results of explosive nucleosynthesis are compared for various initiation methods. In § 6 further studies are made of these initiation methods and their effect upon nickel production. In a final section we discuss these results and our conclusions.

## 2. DEFINING AND INITIATING SHOCK WAVES

When discussing shock waves in presupernova models, one continually refers to the kinetic, internal, and gravitational energy. We begin by defining our usage of these terms. The kinetic energy of the star is given by

$$E_k = \frac{1}{2} \int_0^M dm v^2, \quad (1)$$

where  $v$  is the velocity of the material in the inertial frame and  $M$  is the total mass of the star. The gravitational energy of the star is given by

$$E_g = - \int_0^M dm \frac{Gm}{r}, \quad (2)$$

where  $G$  is the gravitational constant and  $r$  is the radius at the mass point  $m$ . The internal energy is defined as

$$E_i = \int_0^M dm e_i, \quad e_i = \int d\rho \frac{P}{\rho^2}, \quad (3)$$

where  $P$  is the pressure and  $\rho$  is the density. Note that this definition of the internal energy excludes the rest mass of both the electrons and the ions. Since  $Y_e$ , the electron fraction, will not change in the regions we are studying, the electron rest

<sup>1</sup> Present address: Department of Physics and Astronomy, 440 W. Brooks, University of Oklahoma, Norman, OK 73019-0225.

mass energy is an untapped resource. In discussing the gravitational and internal energy of such systems, one must define a zero. Here zero is defined as the case in which the material is infinitely separated from the star. Because the shock wave burns nuclei as it propagates, we must also keep track of the nuclear binding energy released by burning. The nuclear energy is given by

$$E_n = \int_0^M dm N_0 \sum_i \frac{X_i}{A_i} B_i, \quad (4)$$

where  $N_0$  is Avogadro's number,  $X_i$  the mass fraction,  $A_i$  the atomic number, and  $B_i$  the binding energy of the  $i$ th element. The zero for the nuclear energy is defined to be the case in which the nuclei are completely dissociated into free neutrons and protons. Because only a small fraction of the nuclear binding energy is released, most of  $E_n$  is inaccessible and irrelevant to the supernova problem.

In these studies of shock propagation, we use the one-dimensional Lagrangian hydrodynamics code of Baron and Cooperstein (Baron, Cooperstein, & Kahana 1985; Baron 1985). This code employs a numerical scheme which is accurate to second order and uses pseudoviscosity for treating shock waves (Richtmyer & Morton 1967). Although the code can be used in a general relativistic mode, all studies here were Newtonian. Such an approximation has very little effect at the radii with which we are concerned. To the hydrodynamics code has been added an  $\alpha$  nucleus network developed by Thielemann, discussed in detail in Benz, Hills, & Thielemann (1989), so that the energy release due to nuclear burning can be included. In all of the studies discussed in this paper the  $20 M_\odot$  presupernova model for SN 1987A of Nomoto & Hashimoto (1988) is used. It was evolved from a  $6 M_\odot$  He core, and has a  $1.389 M_\odot$  iron core. Table 1 lists the initial contributions to the total energy of the star in column (2). The sum of these energies, the total energy of the star, is  $-1.07$  foe (1 foe is defined as  $10^{51}$  ergs); the star is therefore bound.

A shock wave is defined as a discontinuity in the thermodynamic variables of a fluid, propagating through the medium faster than the speed of sound. Figure 1 shows a situation which is typical for Type II supernovae. As a supernova shock propagates through the star, it compresses and accelerates the material outward. Thus, the material gains kinetic and internal energy from the shock as it passes onward. As the shocked material expands outward, it cools and slows. Although the discontinuity extends over a very small region (microscopic in reality and over several zones in numerical models), the effect of the shock extends from deep within the core out to its present location. How does one define the energy of this shock?

When one starts the shock wave artificially, a definition of the shock is readily apparent. If one compares the total energy

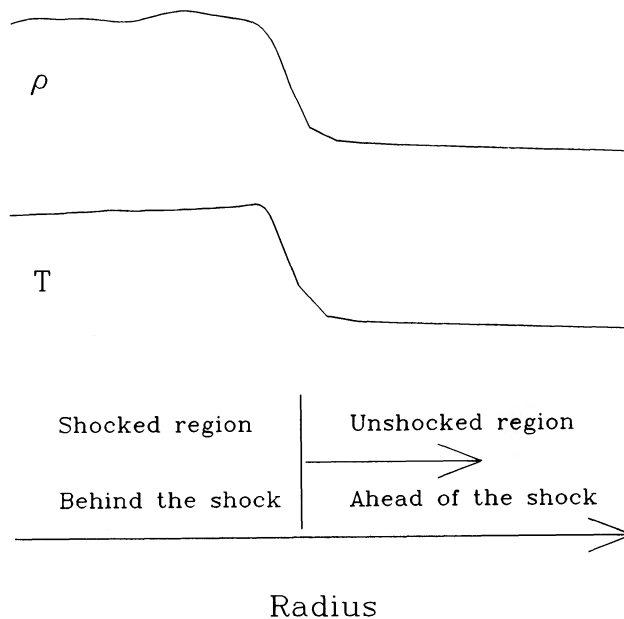


FIG. 1.—Situation typical for shock waves. *Top curve*: density plotted vs. radius. *Lower curve*: temperature plotted vs. radius. In both cases, the discontinuity, softened by pseudoviscosity, is evident. The general situation is displayed below. The shock moves outward, to the right.

of the initial, unshocked model with total energy of the shocked model, the difference in energy will be the shock energy. Thus,

$$E_{\text{shock}} = E_{\text{tot}}|_{\text{mantle}} - E_{\text{tot}}(0)|_{\text{mantle}}, \quad (5)$$

where  $E_{\text{tot}}$  is the sum of  $E_k$ ,  $E_g$ ,  $E_i$ , and  $E_n$ . The “mantle” subscript denotes that we have integrated only over regions affected by the shock wave. Instead of integrating from 0 to  $M$  in equations (1)–(4), we now integrate from  $M_0$  to  $M$ , where  $M_0$  is the mass point of where the shock was started. We have not allowed the core inside  $M_0$  to do any work on the mantle. Except for Table 1, all energies in this paper will refer only to this mantle. Unfortunately,  $E_{\text{shock}}$  is not an energy which can be seen observationally. What is observed is the total kinetic energy of the material ejected from the star,  $E_k(\infty)$ . Some of the material hit by the shock falls back onto the proto-neutron star, carrying some fraction of the shock energy with it. In the case of the artificially induced shocks discussed here, all of the shocked material escapes. Thus, after all the nuclear burning is completed,  $E_k(\infty)$  is the sum of  $E_k$ ,  $E_g$ , and  $E_i$ , and the total energy of the shocked material takes the form

$$E_{\text{tot}} = E_k(\infty) + E_n, \quad (6)$$

where  $E_n$  is the binding energy of the final composition ejected from the star. If we denote the sum of  $E_k(0)$ ,  $E_g(0)$ , and  $E_i(0)$  by  $E_b$  (the additive inverse of the binding energy of the mantle),  $E_{\text{shock}}$  has the following form:

$$E_{\text{shock}} = E_k(\infty) + E_n - E_b - E_n(0). \quad (7)$$

This expression can then be solved for  $E_k(\infty)$ :

$$E_k(\infty) = E_{\text{shock}} + E_b + \Delta E_n, \quad (8)$$

where  $\Delta E_n$  is the nuclear binding energy released by burning. The four quantities in equation (8) are extremely useful for characterizing the initial model and the shock which passes through it.  $E_{\text{shock}}$  is the total energy given to the star by the

TABLE 1

TOTAL ENERGIES FOR EACH INITIAL MODEL

Energy	0 s	0.28 s
(1)	(2)	(3)
$E_k$ .....	+0.00	+0.13
$E_g$ .....	-7.01	-115.11
$E_i$ .....	+5.94	106.62

NOTE.—The total energies of each model are given. All energies are in foe.

shock wave, including nuclear energy release.  $E_k(\infty)$  tells how much kinetic energy will be observed in the ejecta.  $E_b$  tells how strongly the mantle of the initial model is bound to the inner core, and is thus negative.  $\Delta E_n$  shows how much nuclear energy was given to the explosion as a result of the explosive burning.

In the case of a self-consistent calculation, equation (5) will not work, for two reasons. First, there is no shockless initial model with which to compare. In the process of forming the shock wave, the core has collapsed to roughly a tenth of its original radius, and is radiating large amounts of energy in the form of neutrinos. Because the initial model and its later form have become so different, the criterion in equation (5) cannot be used to provide meaningful results. Second, it is not clear until long after the shock has left the star where the mass cut of the supernova will be. Because of this, one cannot determine how much energy actually escapes the star while the shock is still near the edge of the iron core.

Now that the energy of a shock has been defined, we are ready to discuss methods of inducing one. In Figure 2 the three major ways of artificially producing such a shock wave are shown. All three methods subject a region of the star to a violent stimulus which generates a shock wave. In the kinetic energy bomb, a piece of the star is given outward velocities on the order of  $2 \times 10^9$  cm s<sup>-1</sup>. This piece then smashes into the rest of the star, generating a strong shock wave. This approach is not used by any group which models Type II supernova light curves, and so it will not be investigated further.

The second generation method will be called the internal energy bomb (hereafter referred to as a bomb). In this approach, the temperature of a piece of the star is greatly elevated, which increases its pressure and pushes the surrounding material away. The hydrodynamics is set to treat these mass zones as the innermost zones, so that there is expansion outside them but no implosion inward. This ensures that all of the energy initially given propagates outward. The free parameters for the bomb are the initial energy deposited (temperature

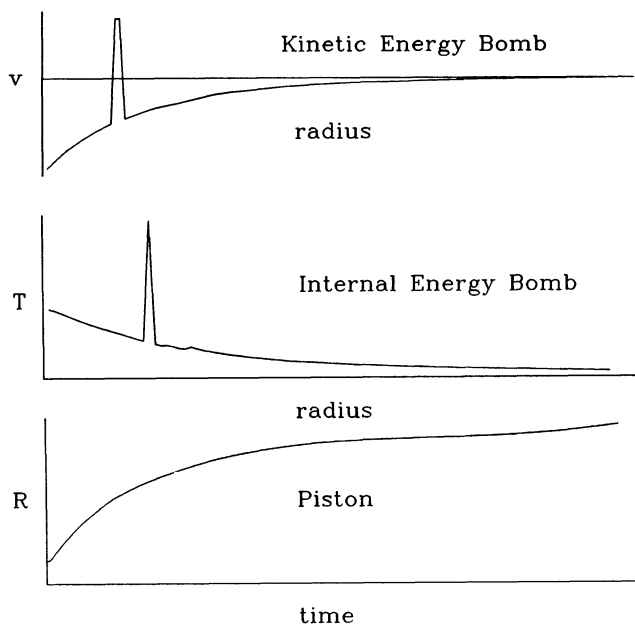


FIG. 2.—Shown are the three main ways of artificially starting a shock wave. In each case the variable which is altered by fiat is plotted against a relevant independent variable.

elevation), the position of this deposition, and the time during the collapse when the bomb is started. This method is used by Nomoto and collaborators (Shigeyama, Nomoto, & Hashimoto 1988; Hashimoto, Nomoto, & Shigeyama 1989; Thielemann, Hashimoto, & Nomoto 1990).

The last method, used by Woosley and Weaver (e.g., Woosley & Weaver 1982, 1986; Woosley 1988; Woosley, Pinto, & Weaver 1988), specifies the motion of one mass point in the star, a “piston.” In current simulations of the light curve and explosive nucleosynthesis of SN 1987A, this piston has been given a ballistic trajectory defined by

$$\frac{du}{dt} = -f \frac{GM_{\text{enc}}}{r^2}, \quad (9)$$

where  $u$  is the velocity of the piston,  $M_{\text{enc}}$  is the mass enclosed by the piston, and  $f$  is a factor which allows us to simulate the reduction in  $G$  due to the pressure gradient within the star. This equation can be integrated to yield

$$u = \begin{cases} \sqrt{u_0^2 + 2fGM_{\text{enc}}(1/r - 1/R_0)}, & r \leq R_{\text{max}}, \\ 0, & \text{otherwise,} \end{cases}$$

where  $u_0$  is the initial velocity given to the piston,  $R_0$  is its initial position, and  $R_{\text{max}}$  is the largest radius the piston reaches before falling back. In actuality, the piston is held at  $R_{\text{max}}$  rather than being allowed to fall back, to avoid the fallback problems listed above. In the models we investigate, nothing outside the piston falls back onto it; everything outside has escaped the star.  $R_{\text{max}}$  is given by the requirement that  $u = 0$  at the maximum radius. One can choose the above parameters so that  $R_{\text{max}} = \infty$ , but this implies that the velocity of the piston is positive at infinity, which can lead to unphysical secondary shocks. We (following Woosley and Weaver) use pistons for which  $R_{\text{max}} < \infty$ .

The piston approach has three free parameters, plus the decision as to when during the collapse to start it. These parameters are  $f$ ,  $M_{\text{enc}}$ , and  $u_0$ .  $R_0$  is determined by the choice of  $M_{\text{enc}}$ . The parameters  $f$  and  $u_0$  determine the energy input to the shock wave. With the piston it is not possible to know *a priori* the energy of the shock wave. The energy is determined by how much work the piston does as it plows into surrounding material. This can only be determined *a posteriori*. This makes the piston somewhat more difficult to use.

In this study, we have used the Nomoto & Hashimoto (1988)  $20 M_{\odot}$  model to compare these two methods of inducing shock waves. We study the initiation of the shock at two times during the collapse of the core: at  $t = 0$  (the initial presupernova model) and after 0.28 s of core collapse. In the collapsed case the initial model was allowed to collapse with completely free-streaming neutrinos (no neutrino trapping at all), until the entire iron core had fallen through the shock wave. In this calculation, the initial model is large enough that the shock wave stalls and becomes an accretion shock. Table 1 lists the total energy of each model. By the later time, the silicon shell is falling inward at velocities ranging from  $0.2 \times 10^9$  cm s<sup>-1</sup> to  $1.4 \times 10^9$  cm s<sup>-1</sup>, and the shock wave has died in the iron core. The silicon shell has started to fall through the remaining accretion shock, dissociating some of the silicon. The iron core radius has shrunk from 1400 to 204 km. Figure 3 shows where the artificial shocks are started and the inner environs of the initial model.

In order to compare shock waves, we have engineered each shock so that  $E_k(\infty)$  has a value of roughly 1 foe, about what is

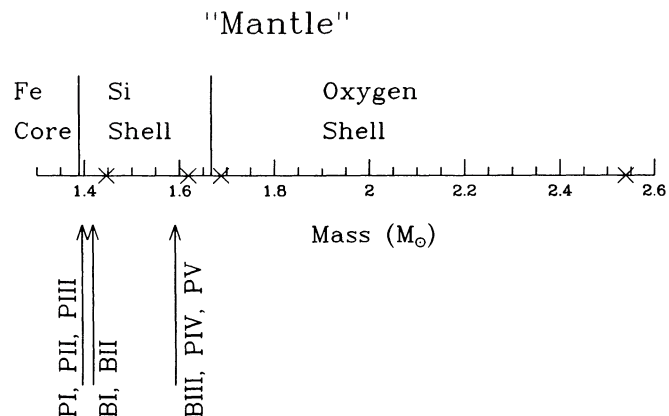


FIG. 3.—Composition of the model used in these studies shown as a function of mass. Crosses denote locations which are discussed in the paper. Arrows point to where various artificial shocks are started.

inferred from light-curve models for SN 1987A (Woosley 1988; Shigeyama, Nomoto, & Hashimoto 1988). In order to obtain 1 foe of energy at the end of the explosion, one needs more than 1 foe when starting the shock. This is because the whole mantle must be ejected. Consider the uncollapsed model. The energy from the shock starting points outward is listed in Table 2 for both shock initiation methods. The mantle of the uncollapsed model is bound by  $-0.56$  ( $-0.59$ ) foies for the bomb (piston). One therefore needs to deposit  $1.56$  ( $1.59$ ) foies in the shock to eject the mantle with 1 foe left over. For the collapsed model, the energies are also listed in Table 2. The shock now needs  $1.95$  ( $2.18$ ) foies in order to unbind the mantle and deliver 1 foe of kinetic energy asymptotically.

A summary of the four cases is given in Table 2. The BI case is a bomb which distributed  $1.57$  foies in one zone at mass point  $1.435 M_{\odot}$  in the uncollapsed model. The energy was deposited in this location by elevating the temperature from  $4.3 \times 10^9$  to  $14.7 \times 10^9$  K, assuming that the region is in nuclear statistical equilibrium. The shock generated in this case has an  $E_k(\infty)$  of  $1.06$  foies. The shock induces a nuclear energy release of  $0.05$  foies. The PI case is a piston placed at the outer edge of the iron core.  $M_{\text{enc}}$  thus has a value of  $1.389 M_{\odot}$ , and the value of  $R_0$  is  $1367$  km. The  $f$ -factor is given a value of unity. Woosley and Weaver typically use a value of  $\frac{1}{2}$ , and this variation will be explored at the end of this section. After choosing  $f = 1$ , it was found that assigning  $u_0$  a value of  $1.63 \times 10^9$  cm s $^{-1}$  created a shock with an energy of  $1.64$  foies and with a value of  $1.12$  foies for  $E_k(\infty)$ . In this case,  $0.06$  foies of nuclear energy was released. The BII case is a bomb which distributed roughly  $1.67$  foies over the same region as BI, but in the collapsed model. In this case the temperature was elevated from  $12.8 \times 10^9$  to  $49 \times 10^9$  K within this region. Note that the deposited energy is less than had been desired above; less energy was needed because the artificial shock passes through a part of the silicon shell which had been dissociated already by the failed shock. After the artificial shock has hit this region, the material will recombine back to iron, releasing several tenths of a foe. This is seen in  $\Delta E_n$ , which now has a value of  $0.31$  foies. The value of  $E_k(\infty)$  is  $1.06$  foies in this case. The PII case is a piston placed at the edge of the iron core in the collapsed model.  $R_0$  now has a value of  $3.041 \times 10^7$  cm, and again  $f$  is chosen to have a value of unity. With this choice of parameters, setting  $u_0$  equal to  $3.72 \times 10^9$  cm s $^{-1}$  has created a shock wave with an energy of

TABLE 2  
RELEVANT INFORMATION ABOUT THE BI, BII, and PI–PIII SHOCKS

0 Seconds of Collapse		0.28 Seconds of Collapse	
Bombs			
Mantle	$\begin{cases} E_k = +0.00 \text{ foies} \\ E_g = -1.44 \text{ foies} \\ E_i = +0.88 \text{ foies} \\ E_b = -0.56 \text{ foies} \end{cases}$	Mantle	$\begin{cases} E_k = +0.12 \text{ foies} \\ E_g = -2.15 \\ E_i = +1.08 \text{ foies} \\ E_b = -0.95 \text{ foies} \end{cases}$
$m > 1.4235 M_{\odot}$		$m > 1.4235 M_{\odot}$	
BI	$\begin{cases} T_9 : 4.3 \rightarrow 14.7 \\ 1.4235 M_{\odot} \leq M \leq 1.435 M_{\odot} \\ E_{\text{shock}} = 1.57 \text{ foies} \\ E_k(\infty) = 1.06 \text{ foies} \\ \Delta E_n = 0.05 \text{ foies} \end{cases}$	BII	$\begin{cases} T_9 : 12.7 \rightarrow 49 \\ 1.4235 M_{\odot} \leq M \leq 1.435 M_{\odot} \\ E_{\text{shock}} = 1.67 \text{ foies} \\ E_k(\infty) = 1.06 \text{ foies} \\ \Delta E_n = 0.31 \text{ foies} \end{cases}$
Pistons			
Mantle	$\begin{cases} E_k = +0.00 \text{ foies} \\ E_g = -1.50 \text{ foies} \\ E_i = +0.91 \text{ foies} \\ E_b = -0.59 \text{ foies} \end{cases}$	Mantle	$\begin{cases} E_k = +0.13 \text{ foies} \\ E_g = -2.53 \text{ foies} \\ E_i = +1.22 \text{ foies} \\ E_b = -1.18 \text{ foies} \end{cases}$
$m > 1.4005 M_{\odot}$		$m > 1.4005 M_{\odot}$	
PI	$\begin{cases} R_0 = 1367 \text{ km}; M_{\text{enc}} = 1.389 \\ u_0 = 1.63 \times 10^9 \text{ cm s}^{-1}; f = 1.0 \\ E_{\text{shock}} = 1.64 \text{ foies} \\ E_k(\infty) = 1.12 \text{ foies} \\ \Delta E_n = 0.06 \text{ foies} \end{cases}$	PII	$\begin{cases} R_0 = 304.1 \text{ km}; M_{\text{enc}} = 1.389 \\ u_0 = 3.72 \times 10^9 \text{ cm s}^{-1}; f = 1.0 \\ E_{\text{shock}} = 1.83 \text{ foies} \\ E_k(\infty) = 1.10 \text{ foies} \\ \Delta E_n = 0.45 \text{ foies} \end{cases}$
Special Piston			
		Mantle	$\begin{cases} E_k = +0.13 \text{ foies} \\ E_g = -2.53 \text{ foies} \\ E_i = +1.22 \text{ foies} \\ E_b = -1.18 \text{ foies} \end{cases}$
		$m > 1.4005 M_{\odot}$	
		PIII	$\begin{cases} R_0 = 304.1 \text{ km}; M_{\text{enc}} = 1.389 \\ u_0 = 2.93 \times 10^9 \text{ cm s}^{-1}; f = 0.5 \\ E_{\text{shock}} = 1.84 \text{ foies} \\ E_k(\infty) = 1.09 \text{ foies} \\ \Delta E_n = 0.44 \text{ foies} \end{cases}$

NOTE.—The relevant information for each comparison case is listed. The top half of each entry contains information about the mantle before the shock is started. The lower half characterizes the shock wave. The temperatures listed for the bombs are in units of  $10^9$  K.

$1.83$  foies, making the final kinetic energy equal to  $1.10$  foies and releasing  $0.45$  foies of nuclear energy.

In Figure 4 the radial position of zone 55 (at  $1.4465 M_{\odot}$  and denoted by a cross in Fig. 3) is plotted as a function of time. As can be seen in Figure 3, this zone is outside the piston by roughly  $0.04 M_{\odot}$  and is just outside the starting point of the bomb. It can be seen that the bomb initially is more violent than the piston in the uncollapsed model. Because of this early difference in trajectories, we expect that the BI peak temperatures should be slightly higher. Greater violence should lead to higher peak temperatures. In the case of the collapsed model, the trajectories are quite similar for the first hundredth of a second, but the piston becomes slightly more violent, driving the zone outward more rapidly. Here we expect the piston to have slightly higher peak temperatures.

All of the pistons discussed above set the parameter  $f$  equal to unity. As was mentioned, Woosley and Weaver typically set  $f$  equal to  $\frac{1}{2}$ . This is because they had wanted to include in some way the  $\partial P/\partial r$  term of hydrodynamics in their trajectory. They

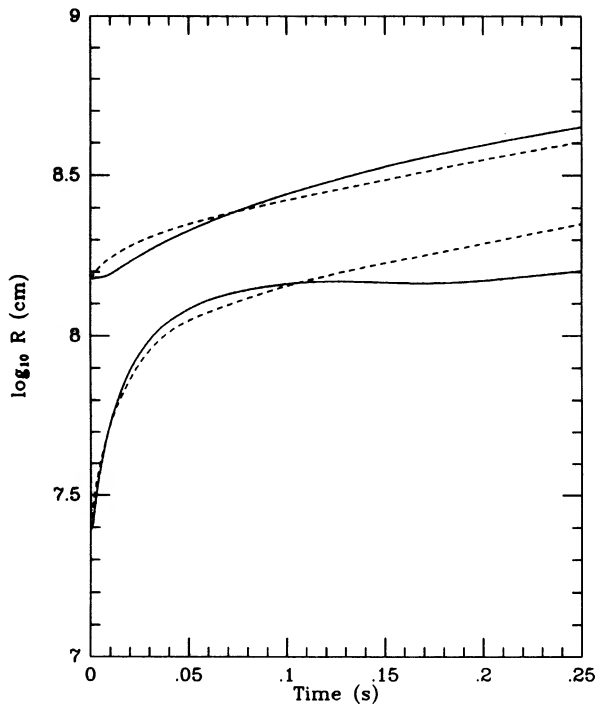


FIG. 4.—Solid lines are trajectories of the zone hit by piston-generated shock waves, while dashed lines are the shocks generated by bombs. The upper two trajectories are in the uncollapsed model; the lower two are in the collapsed model.

saw this gradient as softening the gravitational pull of the inner material. How does the choice of  $f$  affect the piston? Equation (9) shows that reducing  $f$  slows the rate at which the piston decelerates. Thus, if  $u_0$  is fixed, reducing  $f$  will result in a more violent (energetic) piston. The PIII case listed in Table 2 was an exploration of such variations. The same model and piston starting point as in the PII case were used for the PIII shock wave, but  $f$  was chosen to be  $\frac{1}{2}$  for this piston trajectory. The initial piston velocity,  $u_0$ , was then chosen so that  $E_k(\infty)$  was again close to 1 foe. Because  $f$  has been reduced, choosing an initial velocity of  $2.93 \times 10^9 \text{ cm s}^{-1}$  generated a shock which a final kinetic energy of 1.09 foes. This velocity is only 79% of the initial velocity used in PII, yet the shock energies are essentially the same.

### 3. EQUILIBRIUM AND FREEZEOUT

Matter that is initially at high density, once hit by the shock wave, will go into equilibrium. Here we are concerned primarily with the silicon shell, since that is the region of highest densities and temperatures. Once matter is in equilibrium, it is difficult to follow the equilibrium compositions for a long time using rate equations, since the forward and backward rates become extremely large and roughly equal, so that one is attempting to follow the cancellation of large numbers. This is a problem even for implicit differential equation solvers. The obvious solution is to put the material into equilibrium and no longer follow the rate equations. We followed this procedure, and it indeed works quite well. Thus, whenever material in the silicon shell reached a temperature above  $5 \times 10^9 \text{ K}$ , it was put into nuclear statistical equilibrium. This discussion refers only to the silicon shell; in all other parts of the star the rate equations could be followed throughout the entire calculation.

Once the matter has been hit by the shock wave, it expands

and cools adiabatically. Eventually, it reaches a density and temperature such that equilibrium no longer obtains and one must again follow the rate equations. The question now becomes how to follow this freezeout. We investigated two simple methods which both gave approximately the same results, and we chose the smoother method.

One obvious method is to calculate the abundances obtained from the rate equations and to switch over below some specified density and temperature. We chose the value of  $10^6 \text{ g cm}^{-3}$  for this density, and  $T < 10^9 \text{ K}$ . This method leads to a small discontinuity in the temperature, since the equilibrium might be carried beyond its range of applicability. Thus, when we switch back, a sudden energy source or sink could appear. The second method was simply to freeze the abundances at the equilibrium values below some density ( $10^5 \text{ g cm}^{-3}$ ) and temperature ( $T < 10^9 \text{ K}$ ). This method does not introduce any discontinuities, but it may inaccurately estimate the total energy release. In Figure 5 we display the peak temperatures for both methods, and it is clear that, while not identical, the differences between the profiles are rather small. For both these cases the shock was initiated by a bomb on an uncollapsed model. Figure 6 compares the thermal history of zone 70 (at  $1.619 M_\odot$ ), in the outer part of the silicon shell. Here we can clearly see the discontinuity introduced by the first method of freezeout with a sudden switch to the rate equations at  $t = 0.32 \text{ s}$ . It is interesting that this extra shot of energy does not significantly affect the later temperatures once the material has settled down. Figure 5 shows the effect of this release of energy in the peak temperatures near  $2.1 M_\odot$ . In this region, a slight increase in the peak temperatures can be seen relative to the second freezeout treatment. This hump is the result of pressure waves, generated by this small energy release, overtaking and being absorbed by the shock wave. Such phe-

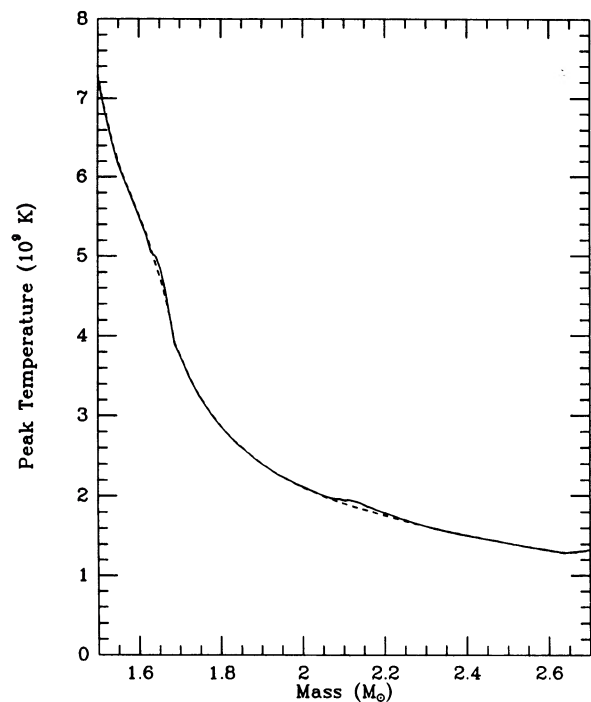


FIG. 5.—Peak temperatures for two different methods of freezeout are compared. The solid line is for the first method discussed in the text and the dashed line for the second. Both calculations used the BI initial conditions.

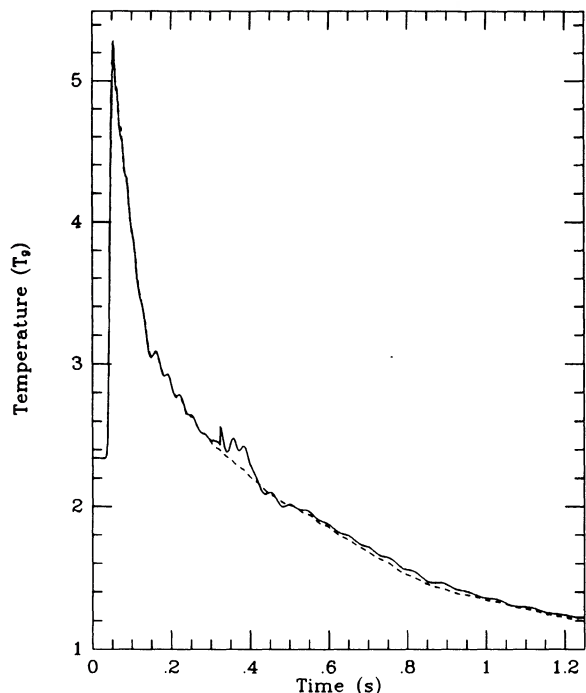


FIG. 6.—Thermal history of zone 70, in the outer part of the silicon shell, for the two freezeout methods. The solid line is for the first method discussed in the text, and the dashed line is for the second. The discontinuity introduced by the first method is evident, although the later temperatures are not much altered.

nomena are common at earlier stages of shock propagation (Brown, Bethe, & Baym 1982).

In principle one would expect a larger binding energy from following an equilibrium network beyond its applicability in comparison with the exact solution of the rate equations, provided that the equilibrium and reaction rate networks contain the same nuclei. Our alpha network is more restricted than our equilibrium network; thus the opposite effect (energy release after switching back to a reaction network) is probably an artifact of this inconsistency. However, the difference between the two methods is small, and we adopted the second method, giving a smooth transition which would result from a correct treatment.

#### 4. COMPARISON OF TEMPERATURE PROFILES

Examining the peak temperatures generated by these shock waves is a good way of comparing their nucleosynthetic yields, since nuclear reaction rates depend exponentially upon the temperature. In Figure 7 the peak temperatures generated by each shock as a function of enclosed mass in the star are plotted. The collapsed models have significantly higher temperatures inside roughly  $1.67 M_{\odot}$  (the silicon shell inward), for two reasons. First, the silicon shell has been compressed somewhat as it followed the collapse of the iron core, leading to higher initial temperatures. Second, the shock hit these zones much more violently because of their larger infall velocities and the greater energy deposited in the shock. It is the second factor which is the more important one, as a look at the initial temperatures in Figure 7 indicates.

For shocks propagating through the uncollapsed model there is a disparity in temperature for  $M \leq 1.625 M_{\odot}$ . The bomb temperatures are higher by roughly 15% at first and

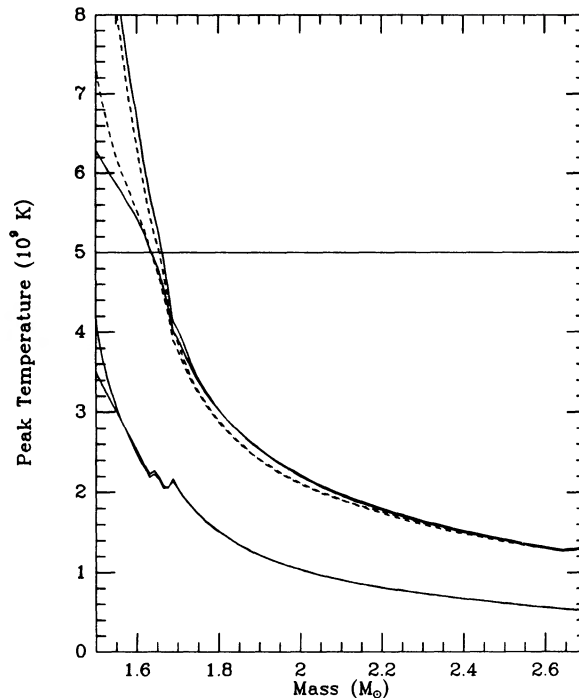


FIG. 7.—The lowest two solid curves are the temperatures for both unshocked initial models. The collapsed model has higher temperatures from  $1.65 M_{\odot}$  inward. The other two solid lines are from the shocks generated by pistons; the dashed lines are from bomb-generated shocks. The two uppermost profiles are the collapsed cases; the middle two curves are the uncollapsed cases.

then converge with the piston's peak temperatures. This behavior is a symptom of one of the dangers of using artificially induced shock waves. Because the bomb starts with all of its energy in internal energy, it will tend to generate temperatures which are unphysically high, until the shock energy has been reasonably partitioned into internal and kinetic energy. The piston starts with its energy as kinetic energy and will thus have temperatures which are too low until the shock energy is properly partitioned. In the collapsed model cases, the shocks have smashed into material so violently that the energy was partitioned much sooner.

In Figure 7 a horizontal line is drawn at a temperature of  $5 \times 10^9$  K. Any material whose peak temperature exceeds this temperature will burn completely to  $^{56}\text{Ni}$ . Thus, the  $^{56}\text{Ni}$  which was seen in SN 1987A must have come from the  $0.07 M_{\odot}$  just inside where the peak temperature drops below  $5 \times 10^9$  K. A more detailed discussion of nickel synthesis, including the effects of incomplete silicon burning, is given in § 5. It can be seen in Figure 7 that the uncollapsed cases agree on where the ejected nickel originated. The collapsed models do not agree as well with one another. The piston makes the nickel  $0.007 M_{\odot}$  farther out than the bomb. Moreover, both collapsed models have the nickel coming from a region at least  $0.02 M_{\odot}$  farther out than do the uncollapsed cases. This difference in position is roughly one-third of the total amount of nickel ejected. It is thus clear that the longer the model collapses before the production of the shock wave, the farther out will the ejected nickel originate.

In Figure 8 the temporal evolution of temperature is plotted at four positions within the star. The  $t = 0$  point is taken as being the time at which each shock is started. Thus, the col-

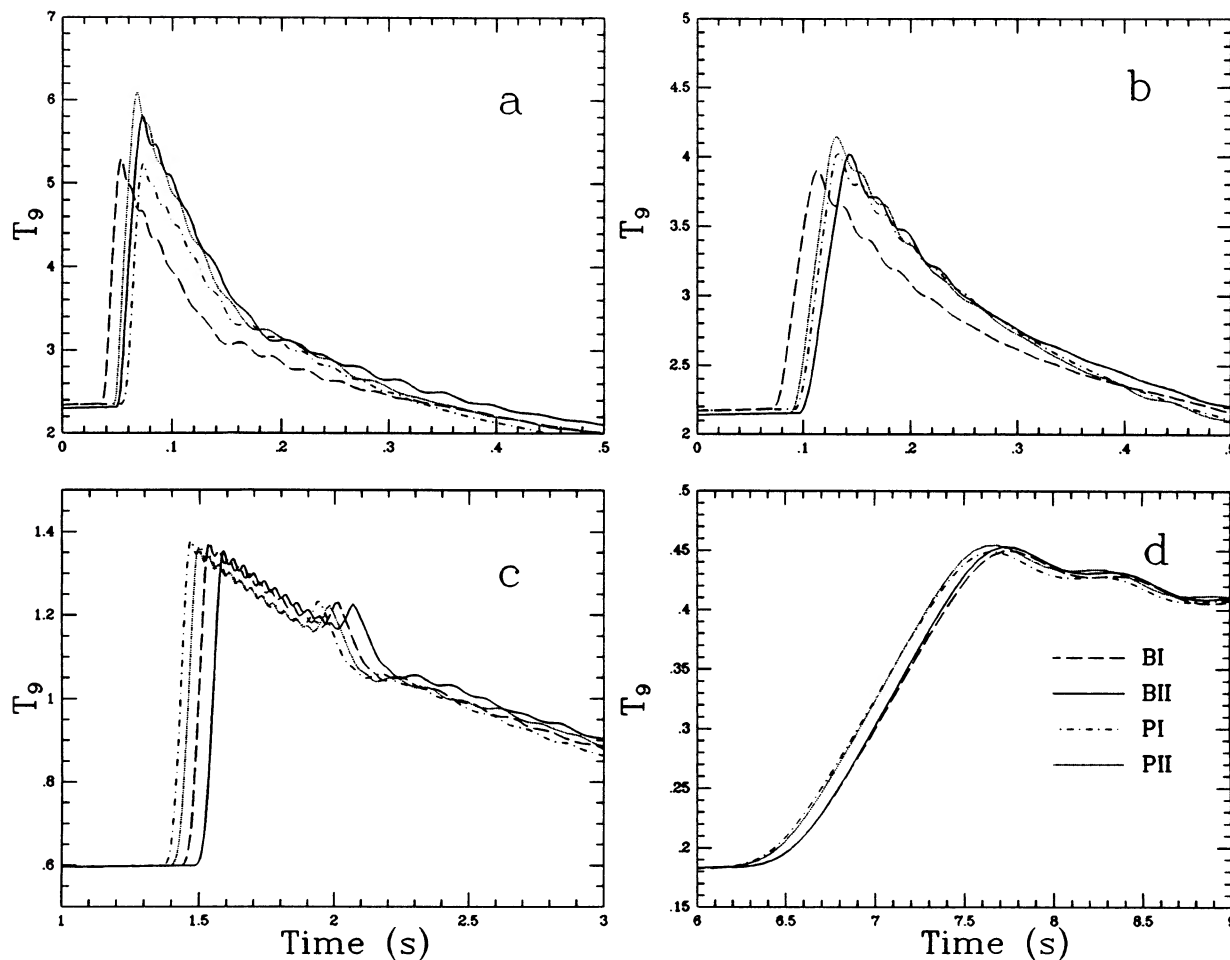


FIG. 8.—The four cases are examined as they hit particular places in the star. The legend in (d) shows the labeling scheme for all four figures. All temperatures are given in  $10^9$  K. The temperature is displayed (a) at  $1.619 M_{\odot}$ , (b) at  $1.688 M_{\odot}$ , (c) at  $2.539 M_{\odot}$ , and (d) at  $3.87 M_{\odot}$ .

lapsed cases are actually 0.28 s later than the uncollapsed ones, although Figures 8a–8d do not show it. Figure 8a corresponds to  $1.619 M_{\odot}$  and is represented as a cross in Figure 3. This point is just inside the outer edge of the silicon shell and would be one of the ejected nickel zones in all four cases. The uncollapsed cases are identical except for the arrival time of the shock. The PI case takes roughly 20 ms longer to reach this point in the star than the BI case. The collapsed cases arrive 5–10 ms earlier than the PI shock. The PII shock is definitely more violent than the BII shock, as the peak temperature and arrival time attest.

Figure 8b shows the temporal evolution at  $1.688 M_{\odot}$ , which also can be seen as a cross in Figure 3. This is the inner edge of the oxygen shell, and it will undergo explosive oxygen burning. Again the BI case arrives first, followed by the PII shock, then the PI shock, and finally the BII shock. The general situation is quite similar to that in Figure 8a, except that the PI shock is catching up with the PII shock. The PII case still has the highest temperature. Note that the BII case has slowed somewhat as compared with other shocks. Figure 8c shows the evolution at an enclosed mass of  $2.539 M_{\odot}$ , which is in the middle of the oxygen shell and also can be seen as a cross in Figure 3. By now the shocks have propagated through enough material that they are approaching a self-similar form, dependent only upon the initial energy input. The PI shock has now

taken the lead, followed by PII, then BI, and finally the BII shock. The temperature profiles are quite similar, although the PII case is now cooler than the originally less violent PI and BI shocks. Note that the piston shocks arrive first and that the shocks on the collapsed model are slightly slower than those on the uncollapsed model. Having to smash through the inwardly falling silicon shell seems to have slowed down the BII and PII shocks. The last set of profiles in this series is that of the  $3.87 M_{\odot}$  mass point, which is the inner edge of the helium shell and is outside the range in Figure 3. This is where explosive helium burning would occur. By now self-similarity has triumphed almost completely. The only major remaining differences are in the arrival times of the bombs relative to the pistons, and this is only a difference of 0.2 s. The differences in peak temperatures at this point are at the 1% level, not large enough to have a significant effect.

From these results it can be seen that the various methods of generating artificial shock waves have some noticeable effects in the silicon shell and beyond. We discuss the detailed differences in the nucleosynthesis in § 5.

When discussing peak temperature profiles, the assumption is often made that the energy of the shock is dominated by radiation. If one assumes uniform temperature and density behind the shock, one can then derive the following expression (Weaver & Woosley 1980) for the peak temperatures experi-

enced by the material as it is shocked:

$$T_p = \left( \frac{3}{4\pi} \frac{E_{\text{shock}}}{ar^3} \right)^{1/4}, \quad (10)$$

where  $a$  is the Stefan-Boltzmann constant and  $r$  is the radius in the initial model for a particular mass point. In Figure 9 this relation is plotted for the uncollapsed model and the collapsed model. In addition the PII and BII temperature profiles are plotted for comparison. This analytic form predicts much higher temperatures than the actual cases until roughly  $2.2 M_\odot$ . The analytic profiles pass through  $T_9 = 5$  roughly  $0.05 M_\odot$  farther out in the model than do the profiles generated by shock waves. From  $1.7 M_\odot$  inward, the peak temperatures estimated for collapsed and uncollapsed models become quite different. This is a result of the much smaller radius of the collapsed iron core and surrounding silicon shell. This difference is slightly reduced because  $T_p$  only goes as  $r^{-3/4}$ . The analytic results and the numeric results are so different at the smaller masses because of the density gradients in the initial models. These gradients are the relics of silicon and oxygen burning. As the shock passes over them, the shocked region is still relatively small in radius, and the internal energy is not yet evenly distributed over the shocked material. Thus the approximation made above is not yet valid. As the shock moves outward in mass, it encloses more and more volume, thus making the perturbations due to these gradients small. After this happens near  $2.2 M_\odot$ , the expression in equation (10) becomes quite accurate.

In Figure 10 peak temperatures are plotted for the BII, PII, and PIII shock waves, so that we can see how the  $f = \frac{1}{2}$  case

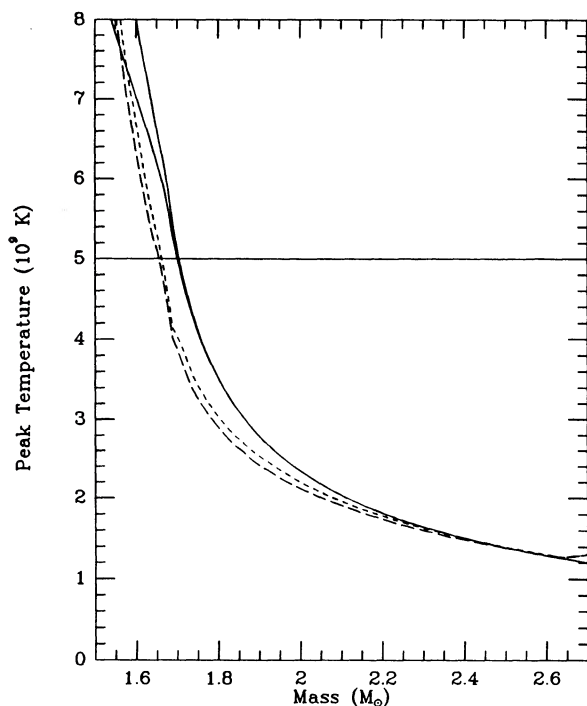


FIG. 9.—Peak temperatures generated by the BII, PII, and analytic expression shocks, plotted as a function of mass. The short-dashed curve is the PII profile, while the long-dashed curve is the BII profile. The two solid curves are profiles resulting from application of eq. (10) to the collapsed and uncollapsed models. The uppermost solid curve corresponds to the collapsed model, and the other solid line is the uncollapsed model.

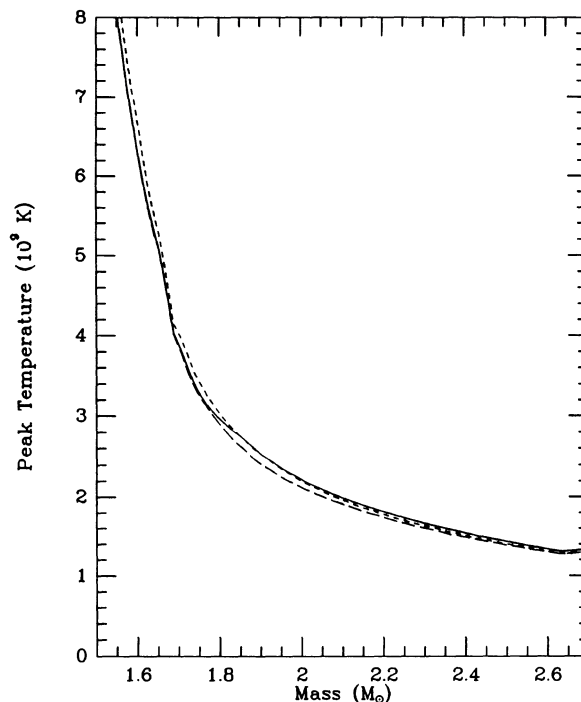


FIG. 10.—Peak temperatures generated by the BII, PII, and PIII shocks are plotted as a function of mass. The solid curve is for PIII, the short-dashed curve is the PII case, and the long-dashed curve is the BII case.

compares with the other two collapsed cases. The behavior of the PIII shock is most amusing. For regions inside roughly  $1.8 M_\odot$ , this piston follows the BII peak temperature profile. But outside  $1.8 M_\odot$  the PIII peak temperature crosses over and becomes similar to the PII profile, although the peak temperatures generated by PIII are higher by roughly 3%. This behavior is surprising because we expect the  $f = \frac{1}{2}$  case to be more violent than the  $f = 1$  case. But the requirement that the asymptotic kinetic energies be comparable has placed a constraint on the pistons. Apparently, if one chooses the final kinetic energy for each kind of shock wave, the  $f = 1$  case is actually slightly more violent. Which case is more violent depends upon what one constrains in the comparison.

#### 5. COMPARISON OF NUCLEOSYNTHETIC RESULTS

The nucleosynthetic results are easily understandable when one examines Figure 7, and they have already been discussed partially in § 4, with respect to the production of  $^{56}\text{Ni}$ . Here we want to give a more general treatment. The nucleosynthesis calculations have been performed in an identical manner to that of Thielemann, Hashimoto, & Nomoto (1990), and further references can be found there. Only a few minor updates of reaction rates of highly unstable targets have been implemented since then. This should not lead to a major change in the outcome. We shall focus mainly on the most abundant alpha nuclei,  $^{12}\text{C}$ ,  $^{16}\text{O}$ ,  $^{20}\text{Ne}$ ,  $^{24}\text{Mg}$ ,  $^{28}\text{Si}$ ,  $^{32}\text{S}$ ,  $^{36}\text{Ar}$ ,  $^{40}\text{Ca}$ ,  $^{52}\text{Fe}$ , and  $^{56}\text{Ni}$ . The detailed production of these nuclei is shown in Figures 11a and 11b. This, however, is only done for a simple discussion of the main features. It can be easily seen which other abundant nuclei are of importance in the individual burning zones from Figures 6, 7, and 8 in Thielemann, Hashimoto, & Nomoto (1990). The abundance and location of the alpha nuclei can be used as a simple indicator for the majority

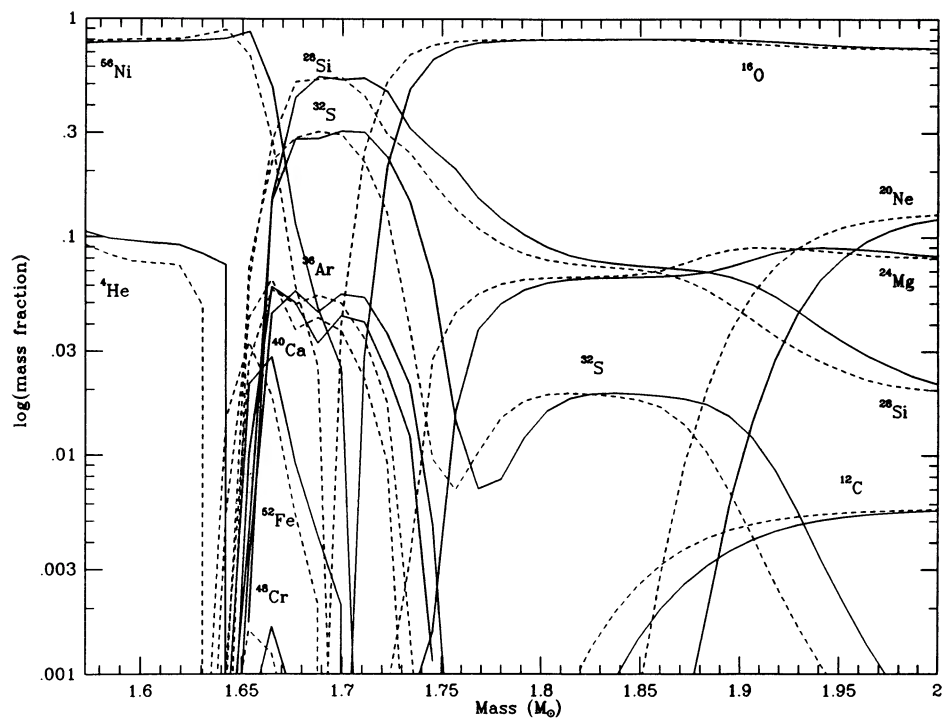


FIG. 11a

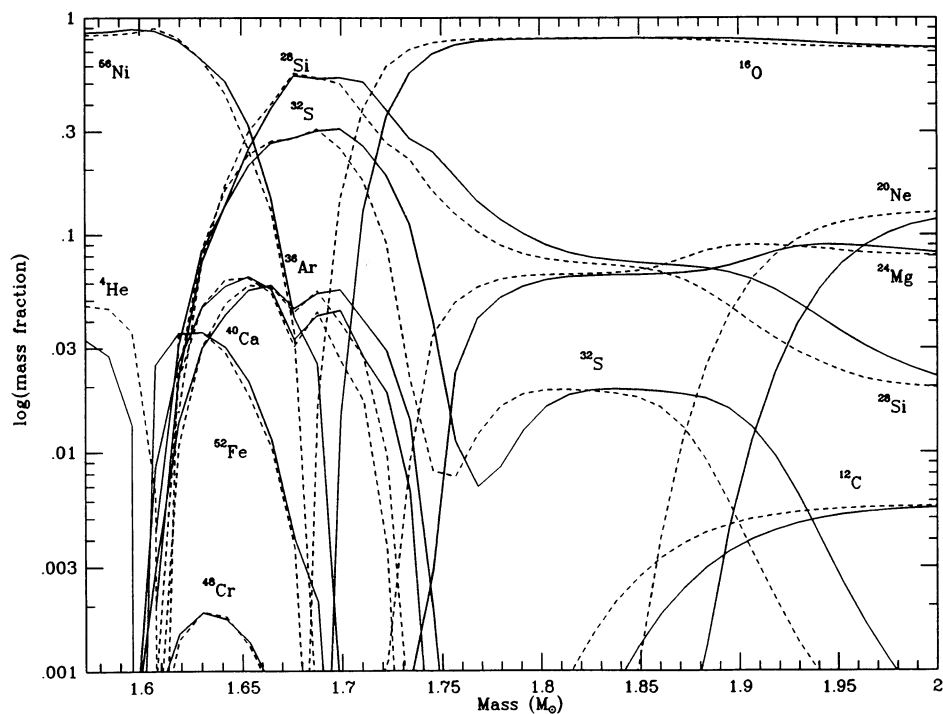


FIG. 11b

FIG. 11.—(a) Abundances for the collapsed model. (b) Abundances for the uncollapsed model. The solid curves correspond to the piston cases, while the dashed curves correspond to the bombs.

of other nuclei. In addition, a more extended set of major abundances is given in Table 3.

At first we want to compare the different results for pistons and bombs. Beyond  $M = 1.675 M_{\odot}$  we find that, for both the collapsed and the uncollapsed models, the pistons result in peak temperatures up to 10% larger than the corresponding internal energy bombs. A complete convergence is only found beyond  $2.2 M_{\odot}$  (see Fig. 7). This means that fuels in the progenitor star are burned out also at larger radii or masses by about 0.01–0.03  $M_{\odot}$  (see the lines for  $^{12}\text{C}$ ,  $^{20}\text{Ne}$ ,  $^{24}\text{Mg}$ , and  $^{16}\text{O}$  in Figs. 11a and 11b for the collapsed and the uncollapsed model, respectively). Accordingly, we find the outer boundary for burning products like  $^{28}\text{Si}$ ,  $^{32}\text{S}$ ,  $^{36}\text{Ar}$ ,  $^{40}\text{Ca}$ ,  $^{52}\text{Fe}$ , and  $^{56}\text{Ni}$  also moved out by comparable amounts. Because the mentioned fuel nuclei are preexisting up to the convergence point beyond  $2.2 M_{\odot}$ , these nuclei are somewhat reduced in the piston calculations. On the other hand, the burning products

$^{28}\text{Si}$  through  $^{56}\text{Ni}$  are produced also in deeper layers inside the “crossing point” at  $1.675 M_{\odot}$  (see Fig. 7). Thus, their total abundance is enhanced in the piston models. This effect is stronger in the uncollapsed initial model than in the collapsed model because the peak temperatures for the piston are smaller inside the crossing point in the uncollapsed model, as opposed to the collapsed case. Consequently, less  $^{28}\text{Si}$  through  $^{52}\text{Fe}$  is transformed into  $^{56}\text{Ni}$  in the uncollapsed models during complete Si burning. In the collapsed model the piston causes higher peak temperatures inside the crossing point, and the gain at larger radii is partly lost at these small radii. Therefore, both effects cancel somewhat. Nevertheless, even in the uncollapsed model the net effect of the differences between pistons and bombs is not large, in no case more than 10%–15%. See for comparison the different columns in Table 3.

Larger differences can be seen between the collapsed and the uncollapsed model, while for each of these models the differ-

TABLE 3  
COMPOSITION OF EJECTED MATERIAL ( $M_{\odot}$ )

Isotope	PI	BI	P11	B11	THN1	THN2	TNH
$^4\text{He}$ .....	2.1E + 00						
$^{12}\text{C}$ .....	1.1E - 01	1.2E - 01					
$^{14}\text{N}$ .....	2.7E - 03	...					
$^{16}\text{O}$ .....	1.5E + 00	1.4E - 01					
$^{18}\text{O}$ .....	8.7E - 03	8.7E - 03	8.7E - 03	8.7E - 03	8.7E + 00	8.7E + 00	...
$^{20}\text{Ne}$ .....	2.3E - 01	2.2E - 01					
$^{21}\text{Ne}$ .....	3.0E - 04	...					
$^{22}\text{Ne}$ .....	2.9E - 02	...					
$^{23}\text{Na}$ .....	1.2E - 03	...					
$^{24}\text{Mg}$ .....	1.5E - 01	1.7E - 01					
$^{25}\text{Mg}$ .....	1.8E - 02	1.9E - 02	1.9E - 02	1.9E - 02	1.8E - 02	1.8E - 02	...
$^{26}\text{Mg}$ .....	1.7E - 02	...					
$^{27}\text{Al}$ .....	1.6E - 02	...					
$^{28}\text{Si}$ .....	9.4E - 02	8.7E - 02	8.7E - 02	8.2E - 02	8.4E - 02	8.4E - 02	9.0E - 02
$^{29}\text{Si}$ .....	1.0E - 02	1.0E - 02	1.0E - 02	1.0E - 02	9.7E - 03	9.7E - 03	...
$^{30}\text{Si}$ .....	7.8E - 03	7.6E - 03	7.7E - 03	7.6E - 03	7.3E - 03	7.3E - 03	...
$^{31}\text{P}$ .....	1.2E - 03	1.2E - 03	1.2E - 03	1.2E - 03	1.1E - 03	1.1E - 03	...
$^{32}\text{S}$ .....	2.9E - 02	2.5E - 02	2.3E - 02	2.1E - 02	2.5E - 02	2.5E - 03	2.5E - 02
$^{33}\text{S}$ .....	1.6E - 04	1.4E - 04	1.5E - 04	1.4E - 04	1.2E - 04	1.2E - 04	...
$^{34}\text{S}$ .....	1.4E - 03	1.2E - 03	1.3E - 03	1.2E - 03	1.1E - 03	1.1E - 03	...
$^{35}\text{Cl}$ .....	6.2E - 05	5.8E - 05	6.0E - 05	5.7E - 05	5.2E - 05	5.2E - 05	...
$^{37}\text{Cl}$ .....	2.2E - 05	2.3E - 05	2.2E - 05	2.2E - 05	6.2E - 06	6.2E - 06	...
$^{36}\text{Ar}$ .....	5.2E - 03	4.5E - 03	3.8E - 03	3.4E - 03	4.1E - 03	4.1E - 03	4.5E - 03
$^{38}\text{Ar}$ .....	4.6E - 04	4.1E - 04	4.0E - 04	3.7E - 04	3.1E - 04	3.1E - 04	...
$^{39}\text{K}$ .....	2.5E - 05	2.3E - 05	2.4E - 05	2.2E - 05	2.9E - 05	2.2E - 05	...
$^{41}\text{K}$ .....	1.8E - 06	1.7E - 06	1.8E - 06	1.7E - 06	2.3E - 06	1.5E - 06	...
$^{40}\text{Ca}$ .....	5.0E - 03	4.3E - 03	3.2E - 03	3.0E - 03	3.3E - 03	3.3E - 03	3.7E - 03
$^{42}\text{Ca}$ .....	1.2E - 05	1.0E - 05	1.0E - 05	9.4E - 06	9.8E - 06	8.4E - 06	...
$^{44}\text{Ca}$ .....	3.2E - 06	6.6E - 06	3.4E - 05	2.4E - 05	2.1E - 04	1.1E - 04	...
$^{46}\text{Ti}$ .....	4.9E - 06	4.4E - 06	4.2E - 06	4.0E - 06	3.7E - 06	3.4E - 06	...
$^{47}\text{Ti}$ .....	1.6E - 07	3.9E - 07	2.0E - 06	1.2E - 06	7.0E - 06	2.8E - 06	...
$^{48}\text{Ti}$ .....	1.0E - 04	9.3E - 05	8.3E - 05	7.1E - 05	2.5E - 04	1.6E - 04	...
$^{49}\text{Ti}$ .....	7.2E - 06	6.5E - 06	3.5E - 06	3.6E - 06	3.8E - 06	3.7E - 06	...
$^{51}\text{V}$ .....	1.4E - 05	1.1E - 05	7.6E - 06	7.3E - 06	1.3E - 05	9.0E - 06	...
$^{50}\text{Cr}$ .....	5.7E - 05	5.0E - 05	3.7E - 05	3.5E - 05	2.9E - 05	2.9E - 05	...
$^{52}\text{Cr}$ .....	1.9E - 03	1.5E - 03	8.1E - 04	8.9E - 04	9.5E - 04	8.4E - 04	...
$^{53}\text{Cr}$ .....	1.8E - 04	1.4E - 04	8.3E - 05	9.1E - 05	8.3E - 05	8.1E - 05	...
$^{55}\text{Mn}$ .....	7.2E - 04	5.2E - 04	3.4E - 04	3.8E - 04	2.8E - 04	2.7E - 04	...
$^{54}\text{Fe}$ .....	5.4E - 03	4.4E - 03	3.1E - 03	3.2E - 03	2.7E - 03	2.7E - 03	...
$^{56}\text{Fe}$ .....	6.4E - 02	6.1E - 02	7.7E - 02	7.3E - 02	7.6E - 02	5.9E - 02	8.0E - 02
$^{57}\text{Fe}$ .....	1.5E - 03	1.7E - 03	2.8E - 03	2.6E - 03	4.2E - 03	2.4E - 03	...
$^{59}\text{Co}$ .....	2.1E - 05	3.0E - 05	7.2E - 05	5.5E - 05	2.0E - 04	8.2E - 05	...
$^{58}\text{Ni}$ .....	2.2E - 03	2.6E - 03	4.1E - 03	3.6E - 03	1.0E - 02	3.8E - 03	...
$^{60}\text{Ni}$ .....	3.3E - 04	6.1E - 04	1.6E - 03	1.3E - 03	2.5E - 03	1.7E - 03	...
$^{61}\text{Ni}$ .....	1.7E - 05	3.4E - 05	9.1E - 05	7.4E - 05	2.3E - 04	1.1E - 04	...
$^{62}\text{Ni}$ .....	1.2E - 04	2.3E - 04	6.3E - 04	5.1E - 04	3.4E - 03	8.8E - 04	...

NOTE.—Composition of ejecta after decay, in solar masses. The integration extends from  $1.675 M_{\odot}$  to the outer edge of the helium shell,  $6 M_{\odot}$ , except for THN1 and THN2, whose mass cuts are at 1.59 and 1.63, respectively.

ences between pistons and bombs is smaller. The difference between uncollapsed and collapsed models only emerges inside  $1.675 M_{\odot}$ , but there the temperature differences can be large. As already discussed in § 4, the boundary between layers with peak temperatures below and above  $5 \times 10^9$  K is moved outward by up to  $0.03 M_{\odot}$ .  $^{56}\text{Ni}$  is, however, also produced in large quantities in incomplete Si burning, whose outer boundary is the same in the collapsed and the uncollapsed model. Therefore, the difference in the total  $^{56}\text{Ni}$  mass is less, about  $0.013 M_{\odot}$ . We also see that these higher temperatures cause a more alpha-rich freezeout (see the  $^4\text{He}$  abundances in Fig. 11). For nuclei like  $^{28}\text{Si}$  and  $^{32}\text{S}$  with mass fractions of about  $2 \times 10^{-1}$  in this affected range from  $1.60$ – $1.65 M_{\odot}$ , the maximum changes in ejected masses are of the order  $5 \times 10^{-3}$ . For the less abundant nuclei these changes decrease accordingly. This can lead to maximum differences in the ejected mass of these intermediate mass nuclei of 30% between the collapsed and the uncollapsed model.  $^{56}\text{Ni}$  can vary by 20%, if we keep the mass cut fixed at  $1.58 M_{\odot}$ .

We come to the following conclusion with regard to different shock initiation methods for supernova nucleosynthesis. Pistons and bombs can lead to results differing up to 10%–15%. Most important, however, is the conceptual question, which initial model should be used for the progenitor star when initiating the shock wave: (1) before collapse, (2) after about 0.28 s, when the central core has collapsed and a stalled shock has formed, or (3) after about 1 s, when a delayed shock powered by neutrinos would form. We found here that about 30% differences can be expected between case 1 and case 2. The results of case 3, i.e., a delayed shock, will be the topic of a future investigation.

It is interesting to compare the present results with the original calculations of Hashimoto, Nomoto, & Shigeyama (1989) and Thielemann, Hashimoto, & Nomoto (1990). It should be stressed here that these calculations made use of a bomb rather than a piston in the uncollapsed  $20 M_{\odot}$  star ( $6 M_{\odot}$ ) of Nomoto & Hashimoto (1988). It turns out, however, that their results are closer to our piston calculation in a collapsed model. This can be seen by comparing with column (5) in Table 3. We give columns (5) and (6) with different mass cuts for historical reasons ( $1.59$  and  $1.63 M_{\odot}$ , respectively). The smaller mass cut gave a more realistic total  $^{56}\text{Ni}$  mass. However, because of too small a  $Y_e$  in the innermost ejected zones, the total amount of stable Ni was largely overproduced. This could only be cured by prohibiting these innermost zones from being ejected and moving the mass cut farther out. The smaller value of  $Y_e = 0.494$  resulted from mixing of Si shell burning products into outer layers. The boundary of this convective layer is, however, very uncertain because of a rather flat entropy distribution. Thus, the dilemma can be solved by extending the  $Y_e$  of 0.498 below  $M = 1.63 M_{\odot}$ , which we did in the present calculations. The final column contains the predictions they derive from an analytical model for the total element abundances (Thielemann, Nomoto, & Hashimoto 1990), using equation (10).

The reason the earlier calculations had more resemblance to a collapsed piston model from our present study might have two possible explanations: (a) the shock wave was initiated too far out and had not fully matured yet, resulting in too high temperatures close to the mass cut between neutron star and ejecta at  $1.6 M_{\odot}$ , and (b) their hydro code (Shigeyama, Nomoto, & Hashimoto 1988) was based on an exact Riemann solver (Yahil, Johnston, & Burrows 1987) which did not make

use of artificial viscosity like the presently used code. In principle, the different hydro codes can lead to 10% differences in peak temperatures due to the smearing out of the shock over several zones, but we do not expect that this is the case here.

It is also interesting to compare our general results with those of Woosley, Pinto, & Weaver (1988). They describe placing their  $f = \frac{1}{2}$  piston at the outer edge of the iron core and generating a shock with  $E_k(\infty)$  of 1.2 foe. Their piston produces  $0.07 M_{\odot}$  of  $^{56}\text{Ni}$ . This result is quite different from those which we have seen in this and the previous section. The PI and PII shocks are both the results of a similar methodology, except with  $f = 1$ . These pistons create over  $0.24 M_{\odot}$  of nickel, hence the reason we place the mass cut relatively far out in the silicon shell. Since they obtained only  $0.07 M_{\odot}$  of nickel from a 1.2 foe piston, without a mass cut somewhere in the silicon shell their peak temperatures must have been much lower than ours. Their calculation used the Woosley and Weaver initial model for SN 1987A (Woosley 1988), while we have employed the Nomoto model. It is possible that the differences we have just discussed are the result of differences between these initial models. If this is the case, then initial model differences could have a greater effect than differences in how or when the shock is started.

## 6. CONCERNING THE EJECTION OF NICKEL

All cases that we have studied possess a serious liability. They eject much more nickel than the supernova does. This overabundance of iron-peak ejecta happens because we have artificially induced shock waves which free all of the material they hit. In § 5 we disregarded this effect and only considered material outside  $M = 1.58 M_{\odot}$ . Using the peak temperature profiles in Figure 7, we could choose a starting point which is just  $0.07 M_{\odot}$  inside the location where  $T_9 = 5$ , and start new shocks with enough energy to provide 1 foe of kinetic energy to the ejecta.

Three such experiments have been performed, and they are listed in Table 4. The PII and BII peak temperature profiles passed through  $T_9 = 5$  at roughly  $1.66 M_{\odot}$ . We therefore start a bomb, an  $f = \frac{1}{2}$  piston, and an  $f = 1$  piston at  $1.59 M_{\odot}$ . These cases are named BIII, PIV, and PV, respectively. Because all three shocks started at the same location, they must overcome the same gravitational binding energy,  $-0.39$  foe. The failed shock wave is inside  $1.59 M_{\odot}$ , so there is no longer any energy release from recombination of shocked nuclei.

The BIII shock was started by raising the temperature of the one zone of the initial model which contained the  $1.59 M_{\odot}$  mass point. This increase was from  $T_9 = 2.51$  to  $T_9 = 10.1$ . The resulting shock wave released 0.06 foe of nuclear energy and had a final kinetic energy of 1.12 foe. The PIV case, with an  $f$ -value of  $\frac{1}{2}$  and an initial piston velocity of  $1.23 \times 10^9$  cm s $^{-1}$ , generated a shock with a total energy of 1.42 foe and a final kinetic energy of 1.05 foe. In this case, only 0.02 foe of nuclear energy were released. This shock seems to have been much weaker than the BIII shock. The PV piston set  $f$  equal to 1 and had an initial velocity of  $1.56 \times 10^9$  cm s $^{-1}$ , 27% faster than the PIV piston, in order to obtain a shock energy of 1.42 foe. Although the shock energies of PIV and PV are the same, the latter shock releases twice the amount of nuclear energy. This indicates that the  $f = 1$  case was a stronger shock than the  $f = \frac{1}{2}$  case. The BIII shock is even stronger, using this criterion.

Figure 12 shows the peak temperatures of these shocks plus the BII and PII profiles for comparison. The amounts of nuclear energy release were a good indication of which case

TABLE 4  
RELEVANT INFORMATION ABOUT THE BIII, PIV, AND PV SHOCKS

0 Seconds of Collapse		0.28 Seconds of Collapse	
Bomb			
Mantle $m > 1.5845 M_{\odot}$		$\begin{cases} E_k = +0.01 \text{ foes} \\ E_g = -1.11 \text{ foes} \\ E_i = +0.71 \text{ foes} \\ E_b = -0.39 \text{ foes} \end{cases}$	
BIII		$\begin{cases} T_9 : 2.51 \rightarrow 10.1 \\ 1.5845 M_{\odot} \leq M \leq 1.596 M_{\odot} \\ E_{\text{shock}} = 1.45 \text{ foes} \\ E_k(\infty) = 1.12 \text{ foes} \\ \Delta E_n = 0.06 \text{ foes} \end{cases}$	
Pistons			
Mantle $m > 1.5845 M_{\odot}$		$\begin{cases} E_k = +0.01 \text{ foes} \\ E_g = -1.11 \text{ foes} \\ E_i = +0.71 \\ E_b = -0.39 \text{ foes} \end{cases}$	
PIV		PV	
$\begin{cases} R_0 = 1864 \text{ km}; M_{\text{enc}} = 1.573 \\ u_0 = 1.23 \times 10^9 \text{ cm s}^{-1}; f = 0.5 \\ E_{\text{shock}} = 1.42 \text{ foes} \\ E_k(\infty) = 1.05 \text{ foes} \\ \Delta E_n = 0.02 \text{ foes} \end{cases}$		$\begin{cases} R_0 = 1864 \text{ km}; M_{\text{enc}} = 1.573 \\ u_0 = 1.56 \times 10^9 \text{ cm s}^{-1}; f = 1.0 \\ E_{\text{shock}} = 1.42 \text{ foes} \\ E_k(\infty) = 1.06 \text{ foes} \\ \Delta E_n = 0.04 \text{ foes} \end{cases}$	

NOTE.—The relevant information for the cases discussed in § 6 is listed, using the same format as in Table 2. All three shocks use the collapsed model. The temperature listed for the bomb is in units of  $10^9$  K. Both pistons have been given initial velocities which exceed the escape velocity for the given parameters. In these models, the piston trajectory was used for only 3 s, after which the piston was held stationary.

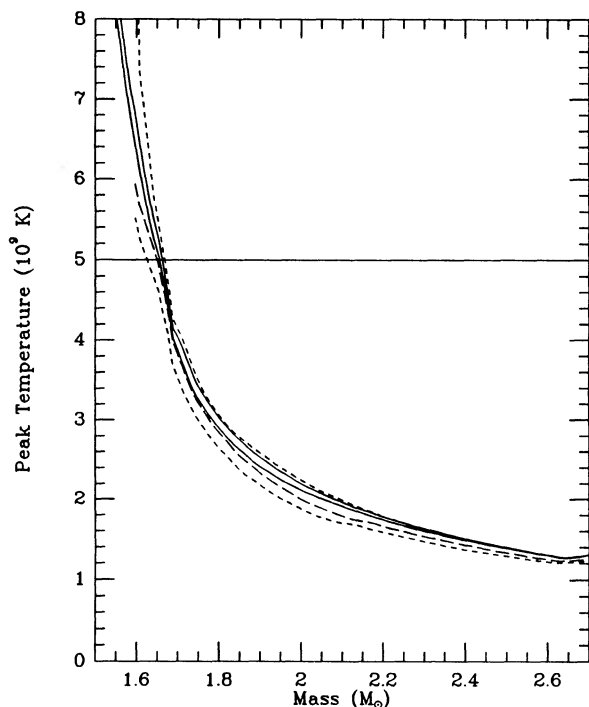


FIG. 12.—The top dashed curve is the BIII case, the long-dashed curve below is the profile generated by the PV shock, and the short-dashed curve, the lowest profile, is the PIV case. The two solid curves are the PII and BII cases, here for comparison with these new cases.

had the higher temperatures. The BIII shock ejects  $0.08 M_{\odot}$  of nickel because its temperatures are so high. The extremely high temperatures inside roughly  $1.75 M_{\odot}$  generated by the bomb are evidence of the immaturity of the shock. In these regions, too much of the shock energy is still internal energy, generating unphysically high temperatures. The pistons show exactly the opposite pathology. Too much of their shock energy is kinetic, generating unphysically low temperatures. This reduces the final yield of nickel. The PV shock ejects  $0.06 M_{\odot}$  of nickel, and the PIV case ejects a paltry  $0.02 M_{\odot}$  of nickel. As was seen in § 4 the  $f = \frac{1}{2}$  piston also generates significantly lower peak temperatures than did the  $f = 1$  case. It can also be seen that both piston-generated shocks must smash through much more material than did the bomb before they approach the profiles of mature shock waves.

None of these cases ejected the correct amount of nickel. One could iterate this process until the correct amount was ejected, but there are two problems with such a procedure. First, each initiation method will decide upon a different starting point. Second, it can be seen in Figure 12 that, near the initiation point, the peak temperatures are unphysical anyway. The region where the nickel is produced is just this region. Thus such an iterative approach is wrongheaded. It will yield a mass cut using unrealistic temperatures. The best that can be done is to start the shocks far enough in so that they are mature by the time they reach the outermost nickel-producing regions.

## 7. CONCLUSIONS

So far we have discussed the peak temperatures assuming that our hydrodynamics gives completely accurate results. One may worry that in particular, the pseudoviscosity smears the shock wave over too many zones and hence underestimates the peak temperatures. We do not believe that this is a major problem in our calculations. First of all, the models are zoned very finely, with  $1/90 M_{\odot}$  per zone in the silicon shell, where we are most concerned about the peak temperatures. Second, Fryxell, Müller, & Arnett (1990) have recently studied the effects of different numerical techniques on the outcome of hydrodynamic burning problems, i.e., on the problem at hand. While their results clearly indicate the Lagrangian piecewise parabolic method to be superior to any of the other methods they study, their results on the Eulerian donor-cell method show that the average values of the temperature in the shock-tube problem are quite good. The main problem with the donor-cell method is that oscillations in the temperature occur. While our method is closest to the donor-cell method, it is a Lagrangian scheme, and the resolution is enhanced over the Eulerian one. Also, in determining the mass of  $^{56}\text{Ni}$  ejected, any oscillations in the temperature will not be that important.

We have examined the peak temperature and nucleosynthetic yields from the two standard methods of shock initiation. It seems clear from our results that one cannot constrain the mass cut to better than about  $0.05 M_{\odot}$  using these results. In addition, any fallback onto the neutron star caused by a reverse shock wave will be an additional uncertainty. The models which were collapsed prior to shock initiation show more differences between “bombs” and pistons. These models better represent the physics that occurs in the supernova problem, since the entire outburst is initially powered by the release of gravitational potential energy during the collapse of the iron core. There is no way to get around the fact that the models should be evolved for some hundreds of milliseconds

after the presupernova models stop the evolution. Thus, these differences make determinations of the mass cut from nucleosynthetic modeling more uncertain. The results from § 5 indicate that we expect up to 10% uncertainties in major abundances from different shock initiation schemes and up to 30% due to the uncertainty when in the collapsing model the shock is initiated. In addition, the possibility that the supernova is powered by a delayed shock wave makes the models all the more suspect. That is because the delayed shock receives energy over a period of several seconds, rather than instantaneously as we have modeled it here. Also, just when the shock wave takes off and how long a model should be collapsed before shock initiation introduces another unconstrained parameter into the models.

The main result of this work is that, with either method of shock initiation, the peak temperatures are incorrect in the early history of the shock. This is because either too much energy is in internal energy, for the case of the bomb, or too much energy is in kinetic energy, in the case of the piston. Thus, the prudent modeler would initiate the shock well inside of the region that he expects the mass cut to be in. This allows the shock wave enough time to partition the energy between internal and kinetic. In addition, it seems that there is little point in attempting to begin a shock wave so that it just ejects the empirically desired amount of  $^{56}\text{Ni}$ , since such a shock wave is far too immature at the initial point.

In spite of these caveats, and especially once the shock wave is past the edge of the silicon shell, either initiation method seems to give good results, and hence one can believe the results for the nucleosynthetic yields and the modeled light curves.

We would like to thank Jerry Cooperstein, Ewald Müller, Ken Nomoto, Toshikazu Shigeyama, Tom Weaver, and Stan Woosley for useful discussions. We would also like to thank Jerry Cooperstein for the use of the hydrodynamical code developed by E. B. and him, and Ken Nomoto and Masa Hashimoto for providing us with the supernova progenitor model of a  $20 M_{\odot}$  star. M. B. A. would also like to thank the Center for Astrophysics, Lick Observatory, and the Special Studies Group of Lawrence Livermore National Laboratory for the kind hospitality which was extended during some of the stages of this work. The calculations reported here were done at the NMFEC at Livermore Laboratory, under the auspices of the Nuclear Physics Division of the US Department of Energy, and at the National Center for Supercomputing Applications at the University of Illinois (AST 890009N). We thank them for a generous allocation of computer time. This work was supported in part by US Department of Energy grant DE-FG02-88ER40388, by NSF grant AST-8913799, and by NASA grant NGR-22-007-272.

#### REFERENCES

- Baron, E. 1985, Ph.D. thesis, SUNY at Stony Brook  
 Baron, E., Cooperstein, J., & Kahana, S. 1985, *Phys. Rev. Letters*, 55, 126  
 Benz, W., Hills, J. G., & Thielemann, F.-K. 1989, *ApJ*, 342, 986  
 Brown, G. E., Bethe, H. A., & Baym, G. 1982, *Nucl. Phys. A*, 375, 481, Appendix C  
 Fryxell, B. A., Müller, E., & Arnett, D. 1990, in *Numerical Methods in Astrophysics*, ed. P. R. Woodward, in press  
 Hashimoto, M., Nomoto, K., & Shigeyama, T. 1989, *A&A*, 210, L5  
 Mayle, R., & Wilson, J. R. 1990, in *Supernovae: Proc. Tenth Santa Cruz Summer Workshop*, ed. S. E. Woosley (New York: Springer-Verlag), in press  
 Nomoto, K., & Hashimoto, M. 1988, *Phys. Repts.*, 163, 13  
 Richtmyer, R. D., & Morton, K. W. 1967, *Difference Methods for Initial-Value Problems* (2d ed.; New York: Wiley)  
 Sedov, L. I. 1959, *Similarity and Dimensional Methods in Mechanics* (New York: Academic Press)
- Shigeyama, T., Nomoto, K., & Hashimoto, M. 1988, *A&A*, 196, 141  
 Thielemann, F.-K., Hashimoto, M., & Nomoto, K. 1990, *ApJ*, 349, 222  
 Thielemann, F.-K., Nomoto, K., & Hashimoto, M. 1990, in *Chemical and Dynamical Evolution of Galaxies*, ed. F. Matteucci and J. Danziger, in press  
 Weaver, T. A., & Woosley, S. E. 1980, *Ann. NY Acad. Sci.*, 336, 335  
 Woosley, S. E. 1988, *ApJ*, 330, 218  
 Woosley, S. E., Pinto, P. A., & Weaver, T. A. 1988, *Proc. Astr. Soc. Australia*, 7 (No. 4), 355  
 Woosley, S. E., & Weaver, T. A. 1982, in *Essays in Nuclear Astrophysics*, ed. C. A. Barnes, D. D. Clayton, & D. N. Schramm (Cambridge: Cambridge Univ. Press), 377  
 ———. 1986, *ARA&A*, 24, 205  
 Yahil, A., Johnston, M. D., and Burrows, A. 1987, unpublished